

# Cross-Attention Transformer for Joint Multi-Receiver Uplink Neural Decoding

Xavier Tardy<sup>1,2</sup>, Grégoire Lefebvre<sup>2</sup>, Apostolos Kountouris<sup>2</sup>, Haïfa Farès<sup>1</sup>, Amor Nafkha<sup>1</sup>

<sup>1</sup>IETR - UMR CNRS 6164, CentraleSupélec, avenue de la Boulaie - CS 47601 35576 CESSON-SEVIGNE Cedex, France

Email: firstname.lastname@centralesupelec.fr

<sup>2</sup>Orange Research, Grenoble, France

Email: firstname.lastname@orange.com

**Abstract**—We propose a cross-attention Transformer for joint decoding of uplink OFDM signals received by multiple coordinated access points. A shared per-receiver encoder learns time–frequency structure within each received grid, and a token-wise cross-attention module fuses the receivers to produce soft log-likelihood ratios for a standard channel decoder, without requiring explicit per-receiver channel estimates. Trained with a bit-metric objective, the model adapts its fusion to per-receiver reliability, tolerates missing or degraded links, and remains robust when pilots are sparse. Across realistic Wi-Fi channels, it consistently outperforms classical pipelines and strong convolutional baselines, frequently matching (and in some cases surpassing) a powerful baseline that assumes perfect channel knowledge per access point. Despite its expressiveness, the architecture is compact, has low computational cost (low GFLOPs), and achieves low latency on GPUs, making it a practical building block for next-generation Wi-Fi receivers.

**Index Terms**—cooperative reception, multi-AP joint decoding, neural receiver, Transformer, channel estimation, WiFi 8, OFDM

## I. INTRODUCTION

The continuing evolution of wireless standards and deployments—exemplified by recent advances in IEEE 802.11be (Wi-Fi 7) and the emerging P802.11bn (Wi-Fi 8) standard [1]—is driving unprecedented demands for throughput, reliability, and multi-link coordination. These trends make cooperative uplink reception a key enabler for improving coverage, mitigating fading, and managing interference for high-order Orthogonal Frequency-Division Multiplexing (OFDM) transmissions. Coordinated multi-AP reception, in the spirit of cell-free [2] or Coordinated Multi-Point (CoMP) architectures [3], exploits geographically diverse observations of the same uplink transmission to enhance spatial diversity and smooth local traffic hotspots. When multiple APs jointly process received OFDM resource grids, they can provide notable gains in bit error rate (BER) and link robustness by coherently combining information across receivers and subcarriers. Recent architectural developments—such as low-latency fronthaul, edge computing, and flexible split-processing—further reduce the implementation barriers for such joint processing. Conventional receiver pipelines, however, remain a limiting factor in realizing these gains. These pipelines typically consist

of three stages: pilot-based channel estimation, equalization, and demapping. Simple estimators like Least Squares (LS) [4] are sensitive to noise, while optimal linear schemes like Linear Minimum Mean Square Error (LMMSE) [5] require accurate second-order channel statistics that are often unavailable or quickly outdated in non-stationary environments. Moreover, performing these steps independently at each AP ignores the spatial correlations that exist between APs and does not adapt the fusion process to the varying reliability of each AP. As a result, significant cooperative gains remain unexploited.

Motivated by these limitations and inspired by the recent successes of machine learning for the physical layer [6]–[8], we investigate learned joint decoding strategies that operate directly on multi-AP OFDM observations. While many data-driven receivers focus on point-to-point links, our work explicitly addresses the multi-receiver fusion challenge. We propose a Transformer-based neural receiver that employs cross-attention mechanisms to capture inter-AP and inter-subcarrier dependencies. In brief, attention assigns data-dependent weights so that each time–frequency position forms a soft, content-aware combination of the most relevant neighbors (with pilots acting as anchors), while cross-attention applies the same principle across APs to achieve a fusion of multi-views. This approach enables scalable, robustness-oriented fusion without requiring explicit per-AP channel state information (CSI). The proposed model aims to: (i) leverage spatial and spectral structure across APs, (ii) tolerate missing or highly degraded links, and (iii) provide a single trainable decoder that outputs soft information log-likelihood ratios (LLRs) suitable for modern channel decoders.

## II. STATE OF THE ART

This section reviews receiver designs for point-to-point uplink OFDM, focusing on decoding reliability and complexity under practical constraints such as sparse pilots, non-stationary channels, and coordinated multi-AP reception.

### A. Classical Estimators: LS and LMMSE

Conventional OFDM receivers estimate the channel from pilots, equalize per subcarrier, and demap to soft information. With a comb or block pilot pattern, the Least Squares (LS) [4] estimator computes per-pilot channel samples by element-wise normalizing the received pilot symbols with

This work was supported in part by Bpifrance under the France 2030 i-Démo program (Wi-FIP project, 2023–2026, Grant I-DEMO-52255).

their known transmitted values and then reconstructs the full time–frequency channel by interpolation across subcarriers and OFDM symbols. LS is unbiased and lightweight but noise-sensitive at low Signal-to-Noise Ratio (SNR) and in interference.

When (approximate) second-order channel/noise statistics are available, Linear Minimum Mean Square Error (LMMSE) estimation reduces the MSE on pilots and, after interpolation, on the full grid [5]. LMMSE gains, however, hinge on covariance knowledge that is often unavailable, device-dependent, or quickly outdated in non-stationary deployments. Moreover, both LS and LMMSE are commonly applied independently per AP, ignoring potential inter-AP spatial correlations carried by the multi-receiver observations.

After channel estimation, model-based equalizers (e.g., Zero-Forcing/MMSE per subcarrier) deliver symbol estimates that are demapped into bit-wise LLRs for the channel decoder. This modular pipeline remains interpretable and standard-compliant, but its performance is limited by pilot density, interpolation bias, and the lack of cross-receiver adaptation in multi-AP reception.

### B. Point-to-Point Data-Driven Receivers

Learned receivers replace some or all model-based blocks with a neural network trained to output soft information directly from the received resource grid. This paradigm can implicitly learn channel estimation, equalization, interference mitigation, and soft demapping.

1) *CNN-based receiver*: Convolutional Neural Networks (CNNs) exploit local time–frequency correlations on the 2D OFDM grid; fully convolutional designs learn to denoise, interpolate, equalize, and demap jointly [6], [7], with complex-valued variants leveraging waveform structure (e.g., cyclic prefix and pilot layout) and end-to-end training reducing pilot overhead without BER loss [9]; in short, they are parameter-efficient and accelerator-friendly but offer limited long-range context and can be fragile under highly selective fades.

2) *LSTM-based receiver*: Long Short-Term Memory (LSTM) receivers process a sequence of time-ordered vectors (e.g., per-subcarrier features per OFDM symbol), maintaining a latent state that tracks channel dynamics and smooths noisy observations [10], which improves robustness to time selectivity and sparse pilots; succinctly, they capture temporal correlation well but incur sequential latency and model wideband frequency dependencies less effectively.

3) *Transformer-based receiver*: Transformers capture long-range, context-dependent interactions via attention [11]; on OFDM grids, self-attention models non-local dependencies and handles masked Resource Elements (REs). Attention-based receivers report robustness and performance gains over MMSE/CNN baselines across diverse multipath profiles through learned positional encodings and context-aware combining [8]; briefly, they offer global context and adaptive reweighting at the cost of attention scaling with the token count, mitigated by patching and shallow stacks.

### C. From per-AP processing to coordinated multi-AP uplink

In coordinated architectures (CoMP/cell-free), geographically diverse observations  $\{\mathbf{Y}^{(r)}\}_{r=1}^{N_R}$  are exploited to improve reliability [2], [3]. A practical baseline runs a point-to-point chain at each AP and fuses symbols or LLRs centrally (unweighted or SNR/noise-based), which is simple but not frequency-selective and ignores inter-AP correlation; fully joint linear processing can exploit such correlation but demands high-rate fronthaul, costly inversions, and accurate joint statistics, challenging scalability and real-time operation [12].

## III. SYSTEM MODEL AND PROBLEM FORMULATION

In this section, we present the system model and problem formulation, and we state the operating assumptions regarding time/frequency synchronization, pilot allocation, and fronthaul characteristics.

### A. Assumptions

- A1: Time and frequency synchronization between the UE and APs is either ideal, or residual offsets are within a small bounded range handled by the receiver.
- A2: Pilot positions (pilot mask) are known a priori and are common to all APs.
- A3: Fronthaul: unless otherwise stated, we assume a low-latency, lossless fronthaul (e.g., optical fiber) that allows centralized processing of raw observations  $\{\mathbf{Y}^{(r)}\}_{r=1}^{N_R}$ , where  $N_R$  is the number of APs.

### B. OFDM Transmission Model

We consider an uplink OFDM transmission scenario where a single-antenna User Equipment (UE) communicates with a set of  $N_R$  coordinated APs, each equipped with a single receive antenna. The transmission spans  $N_c$  subcarriers and  $N_s$  OFDM symbols.

The bitstream  $\mathbf{b} \in \{0, 1\}^k$  is encoded by  $\mathcal{C}(\cdot)$  to produce coded bits  $\mathbf{c} \in \{0, 1\}^n$ . These bits are mapped to complex symbols by the mapper  $\mathcal{M}_c(\cdot)$  and arranged on the OFDM resource grid by  $\mathcal{M}_{rg}(\cdot)$ , yielding:

$$\mathbf{X} = \mathcal{M}_{rg}(\mathcal{M}_c(\mathcal{C}(\mathbf{b}))) \in \mathbb{C}^{N_c \times N_s}, \quad (1)$$

where  $\mathbf{X}$  denotes the transmitted resource grid (subcarrier  $\times$  OFDM symbol).

### C. Channel Model

The wireless channel is modeled according to the 3GPP TR 38.901 specifications for Urban Microcell (UMi) environments [13]. Let  $\mathbf{H} \in \mathbb{C}^{N_c \times N_s}$  denote the channel matrix, where each element  $h_{f,t}$  represents the channel coefficient at subcarrier  $f$  and OFDM symbol  $t$ .

The received signal matrix  $\mathbf{Y} \in \mathbb{C}^{N_c \times N_s}$  is given by:

$$\mathbf{Y} = \mathbf{H} \circ \mathbf{X} + \mathbf{N}, \quad (2)$$

where:

$\mathbf{X} \in \mathbb{C}^{N_c \times N_s}$  is the transmitted resource grid,  $\mathbf{N} \in \mathbb{C}^{N_c \times N_s}$  is the additive white Gaussian noise matrix with entries

$n_{f,t} \sim \mathcal{CN}(0, \sigma_n^2)$ , where  $\sigma_n^2$  is the noise variance,  $\circ$  denotes the Hadamard (element-wise) product.

To enable channel estimation and provide reliable anchors for learning-based receivers, a subset of the resource grid is reserved for known pilot symbols, denoted  $\mathbf{X}_p$ , which are inserted at predefined time-frequency positions (the pilot mask is known a priori and is common to all APs; see A2). On these pilot REs, classical methods estimate the corresponding channel coefficients  $\mathbf{H}_p$  (e.g., LS/LMMSE) and then interpolate/extrapolate across time and frequency to obtain the full channel matrix  $\mathbf{H}$ . The same pilots are exploited by deep learning receivers: presented jointly with neighboring data REs, they act as trusted anchor points that provide sufficient information for the network to infer and compensate for channel-induced amplitude/phase distortions over the grid while producing decoder-ready soft information without requiring explicit per-AP CSI.

#### D. Multi-AP Coordination and Decoding Objective

In a coordinated multi-AP uplink scenario, as illustrated in Fig. 1, a single-antenna UE transmits the signal  $\mathbf{X}$  to  $N_R$  spatially distributed access points. For the  $r$ -th AP, the received signal is:

$$\mathbf{Y}^{(r)} = \mathbf{H}^{(r)} \circ \mathbf{X} + \mathbf{N}^{(r)}, \quad r = 1, \dots, N_R \quad (3)$$

where  $\mathbf{H}^{(r)}$  denotes the UE-to-AP  $r$  channel and  $\mathbf{N}^{(r)}$  the additive noise at AP  $r$  with variance  $\sigma_r^2$ .

The goal of the neural joint decoder is to process the set of received signals  $\{\mathbf{Y}^{(r)}\}_{r=1}^{N_R}$  to produce soft information about the transmitted coded bits  $\mathbf{c}$ . This is formulated as a function  $g_\theta$  parameterized by the learnable weights  $\theta$ , which computes bit-wise log-likelihood ratios (LLRs):

$$\mathbf{L} = g_\theta \left( \{\mathbf{Y}^{(r)}\}_{r=1}^{N_R}, \{\sigma_r^2\}_{r=1}^{N_R} \right) \quad (4)$$

where  $\mathbf{L} \in \mathbb{R}^n$  is the vector of LLRs for the  $n$  coded bits. The function learns to fuse the multi-AP observations without requiring explicit per-AP channel state information (CSI).

We train the joint decoder  $g_\theta$  by maximizing the Bit-Metric Decoding (BMD) rate, denoted by  $R_{\text{BMD}}$ . This objective serves as a differentiable, system-level surrogate for link reliability. In practice, maximizing  $R_{\text{BMD}}$  is strongly correlated with minimizing the BER [9], whereas the BER itself corresponds to a non-differentiable loss. Letting  $s_i \triangleq 2c_i - 1 \in \{-1, +1\}$  be the signed transmitted bits, we solve:

$$\max_{\theta} R_{\text{BMD}}(\theta) = 1 - \frac{1}{n \ln 2} \mathbb{E}_{\mathbf{c}} \left[ \sum_{i=1}^n \log(1 + e^{-s_i L_i}) \right] \quad (5)$$

where the expectation is over the transmitted coded bits  $\mathbf{c}$ .

Maximizing BMD rate is equivalent (up to a constant) to minimizing the average binary cross-entropy (BCE) on the bits:

$$R_{\text{BMD}}(\theta) = 1 - \mathcal{L}_{\text{BCE}}(\theta) \quad (6)$$

Following the neural receiver, the estimated LLRs  $\mathbf{L}_\theta$  are fed into a standard channel decoder. In our case, a Low-density parity-check (LDPC) decoder is used. The decoder

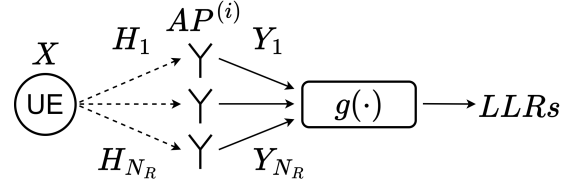


Fig. 1. Neural coordinated decoding with three APs.

processes this soft information to correct errors and produce the final estimate of the information bits,  $\hat{\mathbf{b}}$ . This modular approach allows the neural receiver to act as a drop-in replacement for the conventional chain of channel estimation, equalization, and demapping while leveraging the powerful error-correction capabilities of standard channel codes. The end-to-end performance of the system is then evaluated by comparing the decoded bits  $\hat{\mathbf{b}}$  against the original transmitted bits  $\mathbf{b}$  to compute the BER. For visualization or comparison purposes, an estimate of the transmitted resource grid,  $\hat{\mathbf{X}}$ , can be reconstructed by re-applying the channel coding and modulation scheme to  $\hat{\mathbf{b}}$ .

#### IV. PROPOSED TRANSFORMER-BASED JOINT DECODER

In order to estimate these LLRs, we propose a joint decoder based on a Transformer architecture adapted to multi-receiver OFDM signals. The core idea is to first process each AP received time-frequency grid independently with a shared self-attention encoder to extract local features, and then to fuse these features across all APs using a dedicated cross-attention mechanism. This fusion is performed at the granularity of individual REs, allowing the model to adaptively weight each AP signal for each specific time-frequency bin.

##### A. Network Architecture

The overall architecture, depicted in Fig. 2, consists of three main stages:

- 1) **Per-AP Shared Encoder:** A Transformer encoder with self-attention, shared across all  $N_R$  APs, processes the full Time-Frequency (TF) grid of each receiver independently. It learns to extract a latent representation for each RE, capturing local and global dependencies within that grid.
- 2) **Token-wise Cross-Attention Fusion:** For each TF position  $(f, t)$ , a cross-attention module fuses the  $N_R$  latent representations produced by the encoders. This module learns to dynamically combine information from all APs, effectively up-weighting reliable signals and down-weighting noisy or faded ones.
- 3) **Prediction Head:** A simple Multi-Layer Perceptron (MLP) maps the fused representation of each RE to the corresponding bit-level LLRs.

This design enables scalability with the number of APs and robustness to link failures, as the shared encoder parameters remain constant regardless of  $N_R$ , and the fusion mechanism can learn to ignore missing or corrupted inputs.

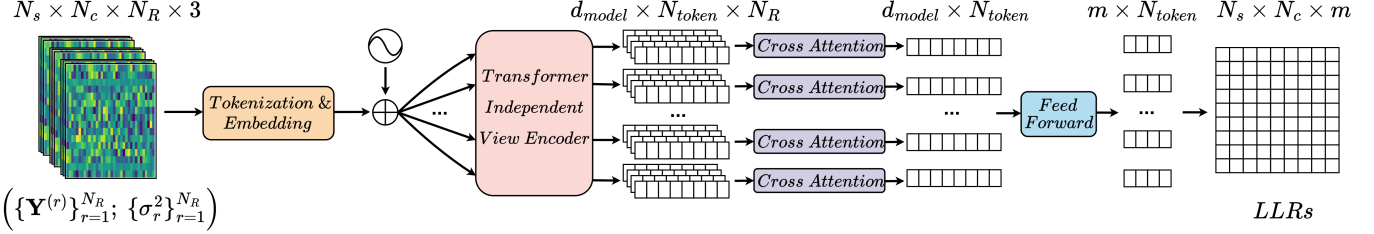


Fig. 2. Architecture of the proposed Transformer joint decoder.

### B. Per-AP Shared Encoder with Self-Attention

For each AP  $r$ , the received complex grid  $\mathbf{Y}^{(r)} \in \mathbb{C}^{N_c \times N_s}$  is first transformed into a sequence of input tokens, yielding a total of  $N_{token} = N_c \times N_s$  tokens. For each RE at subcarrier  $f$  and symbol  $t$ , we form a vector containing the real and imaginary parts of the received symbol and the estimated noise variance at that AP:

$$\mathbf{u}_{f,t}^{(r)} = \begin{bmatrix} \text{Re}(Y_{f,t}^{(r)}) & \text{Im}(Y_{f,t}^{(r)}) & \sigma_r^2 \end{bmatrix}^T \in \mathbb{R}^3. \quad (7)$$

These vectors are treated as  $1 \times 1$  patches. Each token is linearly projected into the model latent dimension  $d_{model}$  and augmented with a 2D sinusoidal positional encoding  $\pi_{f,t}$  to retain its TF position information:

$$\mathbf{z}_{0,f,t}^{(r)} = W_e \mathbf{u}_{f,t}^{(r)} + \pi_{f,t} \in \mathbb{R}^{d_{model}}, \quad (8)$$

where  $W_e$  is a shared embedding matrix.

The resulting sequence of  $N_{token}$  tokens for AP  $r$ , denoted  $\mathbf{Z}_0^{(r)}$ , is fed into a stack of 4 encoder layers. Each layer applies multi-head self-attention (MHSA) to capture dependencies across the entire TF grid. For a given sequence of input embeddings  $\mathbf{Z}$ , the scaled dot-product attention is defined as:

$$\text{Attention}(Q, K, V) = \text{softmax} \left( \frac{QK^T}{\sqrt{d_k}} \right) V, \quad (9)$$

where the queries  $Q$ , keys  $K$ , and values  $V$  are linear projections of the input sequence  $\mathbf{Z}$  (i.e.,  $Q = \mathbf{Z}W_Q, K = \mathbf{Z}W_K, V = \mathbf{Z}W_V$ ). The self-attention mechanism allows the model to learn context-aware representations for each RE by attending to all other REs in the same grid.

### C. Token-wise Anchor-Query Cross-Attention

After the shared per-AP encoder, we perform fusion for each time-frequency position  $(f, t)$  independently. For a given position  $(f, t)$ , we consider the sequence of  $N_R$  output embeddings from the encoders, one for each AP:

$$\mathcal{Z}_{f,t} = (\mathbf{z}_{f,t}^{(1)}, \mathbf{z}_{f,t}^{(2)}, \dots, \mathbf{z}_{f,t}^{(N_R)}). \quad (10)$$

This sequence is treated as a set of  $N_R$  tokens, each of dimension  $d_{model}$ .

Fusion is performed using an anchor-based cross-attention mechanism. We designate AP 1 as the "anchor" without loss of generality (any AP could serve this role), while all views

contribute to the keys and values. The query  $\mathbf{q}_{f,t}$ , keys  $\mathbf{K}_{f,t}$ , and values  $\mathbf{V}_{f,t}$  are computed as follows:

$$\mathbf{q}_{f,t} = \mathbf{z}_{f,t}^{(1)} W_Q \in \mathbb{R}^{1 \times d_k}, \quad (11)$$

$$\mathbf{K}_{f,t} = \mathcal{Z}_{f,t} W_K \in \mathbb{R}^{N_R \times d_k}, \quad (12)$$

$$\mathbf{V}_{f,t} = \mathcal{Z}_{f,t} W_V \in \mathbb{R}^{N_R \times d_v}, \quad (13)$$

where  $W_Q$ ,  $W_K$ , and  $W_V$  are learnable projection matrices, and we assume the sequence  $\mathcal{Z}_{f,t}$  is formatted as a matrix of size  $N_R \times d_{model}$ . The attention output  $\mathbf{a}_{f,t}$  is a weighted sum of the values:

$$\mathbf{a}_{f,t} = \text{softmax} \left( \frac{\mathbf{q}_{f,t} \mathbf{K}_{f,t}^T}{\sqrt{d_k}} \right) \mathbf{V}_{f,t} \in \mathbb{R}^{1 \times d_v}. \quad (14)$$

We then apply a residual connection to the anchor embedding, followed by layer normalization, to obtain the fused representation:

$$\mathbf{z}_{f,t}^{\text{fused}} = \text{LN}(\mathbf{z}_{f,t}^{(1)} + \mathbf{a}_{f,t}) \in \mathbb{R}^{d_{model}} \quad (15)$$

A lightweight MLP finally maps  $\mathbf{z}_{f,t}^{\text{fused}}$  to  $m$  logits (bit LLRs) per RE, where  $m$  is the number of bits per QAM symbol.

$$\mathbf{L}_{f,t} = \text{MLP}(\mathbf{z}_{f,t}^{\text{fused}}) \in \mathbb{R}^m. \quad (16)$$

## V. PERFORMANCE EVALUATION

### A. Simulation Setup

We evaluate the proposed joint decoder against several baselines: classical LS and LMMSE pipelines, a CNN-based receiver from [9], and an ideal per-AP Perfect-CSI demapper. In multi-AP scenarios, these baseline methods first generate Log-Likelihood Ratios (LLRs) independently, which are then centrally fused using SNR-based weighting (i.e., maximal-ratio combining). Simulations follow the 3GPP TR 38.901 Urban Microcell (UMi) channel model to capture realistic multi-path fading. Key parameters are summarized in Table I.

### B. Data Generation

To ensure the model generalizes across diverse channel conditions and avoids overfitting, both training and evaluation data are generated on-the-fly. For each sample, a new scenario is created by randomly placing the single-antenna UE and the  $N_R$  single-antenna APs within a  $25m \times 25m$  square area. The entire simulation pipeline is implemented using the **Sionna** library [14], which provides tools for link-level simulation.

TABLE I  
SIMULATION PARAMETERS

Parameter	Value
Carrier Frequency	2.4 GHz
Bandwidth	20 MHz
Subcarrier Spacing	15 kHz
FFT Size	1024
Number of Subcarriers ( $N_c$ )	48
Number of OFDM Symbols ( $N_s$ )	36
Modulation ( $m = 6$ )	64-QAM
Channel Coding	LDPC 3/4
Channel Model	3GPP TR 38.901 UMi
UE Speed	0-3 m/s
Number of APs ( $N_R$ )	1-3

### C. Experimental Protocol

**Training:** The proposed Transformer-based joint decoder is trained for 30,000 steps using the Adam optimizer. A batch size of 16 is used, where each item in the batch corresponds to a full multi-AP observation  $\{\mathbf{Y}^{(r)}\}_{r=1}^{N_R}$  from an independently generated random topology. The neural network models are built and trained using **TensorFlow** on an NVIDIA RTX 4090 (24 GB).

**Evaluation:** We compute BER using 5,000 Monte Carlo iterations. In every iteration, a random UE/AP placement is generated, and a batch of 16 independent resource grids is transmitted. Each iteration is evaluated at the mean  $E_b/N_0$  across the  $N_R$  receive links and yields one BER sample at that  $E_b/N_0$ . To reduce run-to-run variability, we repeat the entire evaluation 5 times with independent random seeds and report the mean BER across the five runs. The final BER curve is then smoothed using kernel smoothing with a 1 dB bandwidth.

### D. Hyperparameters

All Transformer blocks (shared encoder and cross-attention fusion) use  $d_{\text{model}} = 64$ , 8 heads, 4 layers, a feed-forward network dimension of 128, and a patch size of  $1 \times 1$  (per RE). These values were determined through ablation studies across different numbers of heads, layers, and model dimensions.

### E. Results and Analysis

1) *BER Performance:* Results are shown in Fig. 3 as BER versus the average  $E_b/N_0$  across the  $N_R$  receive links. We assess (i) the impact of cooperation by varying the number of coordinated APs  $N_R \in \{1, 2, 3\}$ , and (ii) robustness to pilot density using two pilot configurations: a “Kronecker-like” pattern with two pilot columns at OFDM symbol indices 2 and 32, and a sparser setting with a single pilot column.

**Impact of Multi-AP Cooperation:** As anticipated, increasing the number of cooperating APs ( $N_R$ ) provides a significant spatial diversity gain, improving the BER performance for all methods. This is evident by comparing the plots column-wise: for a target BER of  $10^{-6}$ , moving from  $N_R = 1$  to  $N_R = 3$  (with 2 pilot columns) reduces the required  $E_b/N_0$  by approximately 7 dB for the Transformer, demonstrating its ability to effectively exploit the additional spatial information.

TABLE II  
COMPUTATION COST PER INFERENCE PASS (GFLOPs)

Method	Parameters	GFLOPs
LS + Eq.+ Demap	N/A	$7.20 \times 10^{-6}$
LMMSE + Eq.+ Demap	N/A	$5.04 \times 10^{-2}$
CNN	8.26 M	$1.33 \times 10^1$
Transformer (Ours)	0.15 M	$2.43 \times 10^{-1}$

**Robustness to Pilot Sparsity:** The comparison between the top row (2 pilot columns) and the bottom row (1 pilot column) highlights the receivers robustness to reduced pilot density. While all methods experience performance degradation, the proposed Transformer shows remarkable resilience. For instance, at  $N_R = 2$ , the Transformer performance with a single pilot column is nearly identical to its performance with two, and it still significantly outperforms the LMMSE and CNN baselines. This suggests that the self-attention mechanism effectively learns to interpolate the channel over long time-frequency distances, making it highly suitable for pilot-sparse scenarios. In contrast, the CNN, which relies on local convolutions, suffers a more noticeable performance drop. In terms of spectral efficiency, reducing the pilot mask from two to a single column increases the fraction of data REs from 34/36 to 35/36, i.e., a relative gain of 2.94%.

**Comparative Performance:** Across all configurations, the proposed Transformer consistently outperforms the LS, LMMSE, and CNN-based receivers. In the single-AP case ( $N_R = 1$ ) with two pilot columns, the Transformer is only 1 dB away from the Perfect-CSI bound, matches LMMSE performance, and outperforms LS and the CNN. As more APs are added, the Transformer closes the gap to the Perfect-CSI reference and, in some cases, even surpasses it. For  $N_R = 3$  with two pilot columns, it is about 1 dB better at medium/high  $E_b/N_0$  than the Perfect-CSI (per-AP) with SNR fusion baseline. The mean standard deviation in this configuration across BER points is 0.3 dB, confirming the stability of these gains. This indicates that cross-attention learns data-dependent, per-RE, AP-adaptive fusion that exploits inter-AP correlation and frequency selectivity beyond fixed SNR weighting.

2) *Computational complexity and Inference time:* The protocol involves 100 inference passes (batch size of 1) to gather stable statistics. For classical methods, this measures the channel estimation, equalization, and demapping stages. For neural models, it measures the forward pass.

**Computational Complexity:** As shown in Table II, the proposed Transformer is remarkably efficient in terms of model size and theoretical operations. With only 0.15M parameters and 0.24 GFLOPs, it is over 50 times smaller and requires 55 times fewer FLOPs than the CNN baseline (8.26M parameters, 13.3 GFLOPs). This highlights the parameter efficiency of the attention mechanism for this task compared to deep convolutional stacks. Both LS and LMMSE have negligible computational costs in comparison.

**Inference latency:** The practical inference performance

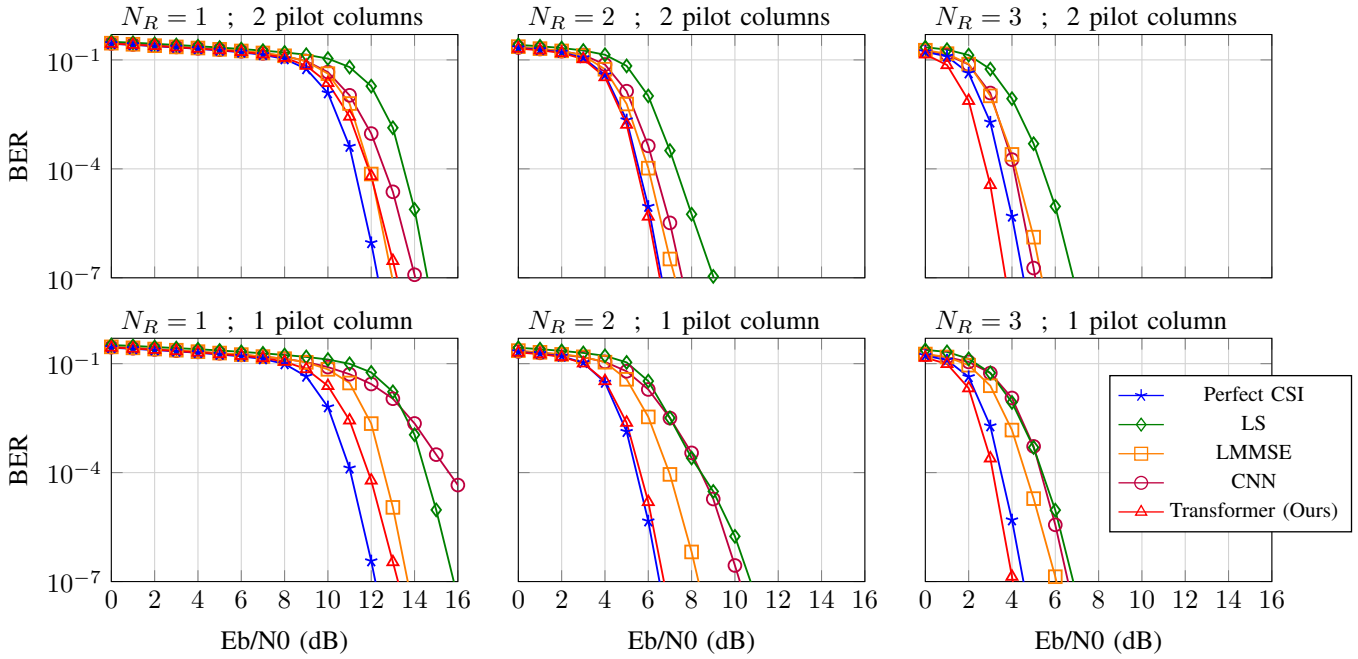


Fig. 3. BER performance vs. Eb/N0 for varying cooperation levels ( $N_R = 1, 2, 3$ ) and pilot configurations (1 vs. 2 pilot columns)

TABLE III  
INFERENCE LATENCY (MEAN  $\pm$  STD, MS)

Method	CPU		GPU	
	$N_R = 1$	$N_R = 3$	$N_R = 1$	$N_R = 3$
LS + Eq.+ Demap	48 $\pm$ 01	165 $\pm$ 11	60 $\pm$ 01	179 $\pm$ 04
LMMSE + Eq.+ Demap	89 $\pm$ 04	276 $\pm$ 05	110 $\pm$ 02	306 $\pm$ 02
CNN	62 $\pm$ 03	152 $\pm$ 07	4 $\pm$ 03	11 $\pm$ 01
Transformer (Ours)	267 $\pm$ 14	639 $\pm$ 03	5 $\pm$ 01	12 $\pm$ 01

is summarized in Table III. On CPU (AMD Ryzen 5 PRO 7530U), the Transformer exhibits the highest latency due to the sequential nature of attention computations; the classical methods and the CNN are faster on this platform. On GPU (NVIDIA RTX 4090 24GB), both the CNN and the Transformer benefit from massive parallelism and achieve single-digit millisecond latency, making them suitable for real-time deployment. Latency increases with  $N_R$  for all methods, but the scaling remains acceptable for the evaluated configurations.

## VI. CONCLUSION AND PERSPECTIVES

We presented a cross-attention Transformer for joint multi-AP uplink decoding that learns intra-grid dependencies per AP and performs token-wise fusion across APs to output LLRs without explicit CSI. Simulations with 3GPP TR 38.901 UMi channels show consistent gains over LS/LMMSE and a strong CNN, resilience to sparse pilots, and performance approaching Perfect-CSI as cooperation increases. The model is compact (0.15M parameters, 0.24 GFLOPs) and offers a favorable performance/complexity trade-off. Future work includes: (i) multi-user extensions addressing interference, (ii) efficiency via linear/axial attention and model compression,

(iii) fronthaul-aware feature sharing and robustness to asynchrony, (iv) blind operation with topology prior.

## REFERENCES

- [1] “P802.11bn - Enhancements for Ultra High Reliability (Project page / PAR),” 2024, published: IEEE 802.11 PARs / Working Group page.
- [2] H. Q. Ngo, E. G. Larsson, and T. L. Marzetta, “Cell-Free Massive MIMO: Foundations and Key Results,” *arXiv preprint*, 2017.
- [3] D. Gesbert, S. Hanly, H. Huang, S. Shamai, O. Simeone, and W. Yu, “Multi-cell MIMO cooperative networks: A new look at interference,” *Journal on Selected Areas in Communications*, vol. 28, no. 9, 2010.
- [4] J. J. van de Beek, O. Edfors, M. Sandell, S. K. Wilson, and P. O. Börjesson, “On channel estimation in ofdm systems,” in *Proceedings of the IEEE Vehicular Technology Conference (VTC)*, 1995.
- [5] M. Biguesh and A. B. Gershman, “Training-based MIMO channel estimation: A study of estimator tradeoffs and optimal training signals,” *IEEE Transactions on Signal Processing*, vol. 54, no. 3, 2006.
- [6] H. Ye, G. Y. Li, and B.-H. Juang, “Power of Deep Learning for Channel Estimation and Signal Detection in OFDM Systems,” *IEEE Wireless Communications Letters*, vol. 7, no. 1, pp. 114–117, Feb. 2018.
- [7] M. Honkala, D. Korpi, and J. M. J. Huttunen, “DeepRx: Fully Convolutional Deep Learning Receiver,” Jan. 2021, *arXiv:2005.01494 [eess]*.
- [8] Y. Xie, K. C. Teh, and A. C. Kot, “Comm-Transformer: A Robust Deep Learning-Based Receiver for OFDM System Under TDL Channel,” *IEEE Transactions on Communications*, vol. 72, no. 4, 2024.
- [9] F. Aït Aoudia and J. Hoydis, “End-to-end learning for ofdm,” *IEEE Transactions on Wireless Communications*, 2022.
- [10] T. O’Shea and J. Hoydis, “An introduction to deep learning for the physical layer,” *IEEE Transactions on Cognitive Communications and Networking*, 2017.
- [11] A. Vaswani, N. Shazeer, N. Parmar, J. Uszkoreit, L. Jones, A. N. Gomez, Ł. Kaiser, and I. Polosukhin, “Attention is all you need,” in *Advances in Neural Information Processing Systems (NeurIPS)*, 2017.
- [12] E. Björnson and L. Sanguinetti, “Scalable cell-free massive mimo systems,” *IEEE Transactions on Communications*, 2020.
- [13] “TR 138 901 - V16.1.0 - 5G; Study on channel model for frequencies from 0.5 to 100 GHz (3GPP TR 38.901 version 16.1.0 Release 16),” Tech. Rep.
- [14] NVIDIA, “Sionna: An open-source library for link-level data-driven wireless communications research,” <https://github.com/nvlab/sionna>.